Multicomponent polariton superfluidity in the optical parametric oscillator regime

A. C. Berceanu,[1] L. Dominici,[2,3,*] I. Carusotto,[4] D. Ballarini,[2,3] E. Cancellieri,[5] G. Gigli,[2] M. H. Szymańska,[6] D. Sanvitto,[2] and F. M. Marchetti[1,†]

[1]*Departamento de Física Teórica de la Materia Condensada & Condensed Matter Physics Center (IFIMAC),*
Universidad Autónoma de Madrid, Madrid 28049, Spain
[2]*CNR NANOTEC - Istituto di Nanotecnologia, Via Monteroni, 73100 Lecce, Italy*
[3]*Istituto Italiano di Tecnologia, IIT-Lecce, Via Barsanti, 73010 Lecce, Italy*
[4]*INO-CNR BEC Center and Universitá di Trento, via Sommarive 14, I-38123 Povo, Italy*
[5]*Department of Physics and Astronomy, University of Sheffield, Sheffield S3 7RH, United Kingdom*
[6]*Department of Physics and Astronomy, University College London, Gower Street, London WC1E 6BT, United Kingdom*

Superfluidity, which is the ability of a liquid or gas to flow with zero viscosity, is one of the most remarkable implications of collective quantum coherence. In equilibrium systems such as liquid ^{4}He and ultracold atomic gases, superfluid behavior conjugates diverse yet related phenomena, such as a persistent metastable flow in multiply connected geometries and the existence of a critical velocity for frictionless flow when hitting a static defect. The link between these different aspects of superfluid behavior is far less clear in driven-dissipative systems displaying collective coherence, such as microcavity polaritons, which raises important questions about their concurrency. With a joint theoretical and experimental study, we show that the scenario is particularly rich for polaritons driven in a three-fluid collective coherent regime, i.e., a so-called optical parametric oscillator. On the one hand, the spontaneous macroscopic coherence following the phase locking of the signal and idler fluids has been shown to be responsible for their simultaneous quantized flow metastability. On the other hand, we show here that the pump, signal, and idler have distinct responses when hitting a static defect; while the signal displays modulations that are barely perceptible, the ones appearing in the pump and idler are determined by their mutual coupling due to nonlinear and parametric processes.

PACS number(s): 03.75.Kk, 71.36.+c, 42.65.Yj

I. INTRODUCTION

Microcavity polaritons, which are the quasiparticles resulting from the coherent strong coupling between quantum-well excitons and cavity photons [1], have unique mixed matter-light properties that none of their constituents displays on its own. Because of their energy dispersion and their strong nonlinearity inherited from the excitonic components, polaritons continuously injected by an external laser into a pump state with suitable wave vector and energy can undergo coherent stimulated scattering into two conjugate states [2–4], namely the signal and the idler, a process known as optical parametric oscillation (OPO). Since their first realization [5–9], the interest in microcavity optical parametric phenomena has involved several fields of fundamental and applicative research [10–16].

Recently, considerable resources have been invested in exploring the fundamental properties of parametric processes, including the possibility of macroscopic phase coherence and superfluid behavior [17]. In spite of the coherent nature of the driving laser pump, the OPO process belongs to the class of nonequilibrium phase transitions in which a U(1) phase symmetry is spontaneously broken [18]. While the phase of the pumped mode is locked to the incident laser, the phases of the signal and idler are free to be simultaneously rotated in opposite directions. Because of

this phase freedom, recent experiments [19] have tested the OPO superfluid properties by exploring the physics of the signal-idler order parameter, demonstrating the existence and metastability of vortex configurations. As the order parameter involves both the signal and the idler, their phase winding have opposite signs [19–21]. Crucially, this causes both OPO fluids to display quantized flow metastability simultaneously.

While in equilibrium condensates different aspects of superfluidity are typically closely related [22], this is no longer true in a nonequilibrium context such as for microcavity polaritons [17]. In particular, those aspects of superfluidity related to frictionless flow around defects are expected to be much more involved in OPO condensates than for any other investigated polariton condensates, such as for the case of incoherent pumping [23,24] and single-state resonantly pumped microcavities [25]. Independent of the pumping scheme, the driving and the polariton finite lifetime prompt questions about the meaning of superfluid behavior when the spectrum of collective excitations is complex rather than real, raising conceptual interrogatives about the applicability of a Landau criterion [24]. However, an additional complexity characterizes the OPO regime, i.e., the simultaneous presence of three oscillation frequencies and momenta for the pump, signal, and idler correspondingly multiplies the number of collective excitation branches [18]. Note that from an experimental point of view, pioneering experiments [26] have observed a ballistic nonspreading propagation of signal/idler polariton wave packets in a triggered-OPO configuration. However, given the complexity of the dynamics as well as the nonlinear interactions involved in this time-dependent configuration

*lorenzo.dominici@gmail.com
†Author to whom all correspondence should be addressed: francesca.marchetti@uam.es

[27], a theoretical understanding of these observations is not complete yet.

This article reports a joint theoretical and experimental study of an OPO configuration in which a wide and steady-state condensate hits a stationary localized defect in the microcavity. Contrary to the criterion for quantized flow metastability for which the signal and idler display simultaneous locked responses, we find that their scattering properties when the OPO hits a static defect are different. In particular, we investigate the scattering properties of all three fluids, the pump, the signal, and the idler, in both real and momentum space. We find that the modulations generated by the defect in each fluid are not only determined by its associated Rayleigh scattering ring, but each component displays additional rings because of the cross-talk with the other components imposed by nonlinear and parametric processes. We single out three factors determining which one of these rings has the biggest influence on each fluid response: the coupling strength between the three OPO states, the resonance of the ring with the blueshifted lower polariton dispersion, and the values of each fluid group velocity and lifetime together establishing how far each modulation can propagate from the defect. The concurrence of these effects implies that the idler strongly scatters inheriting the same modulations as the pump, while the modulations due to its own ring can propagate only very close to the defect and cannot be appreciated. However, the modulations in the signal are strongly suppressed and not at all visible in experiments because the slope of the polariton dispersion in its low momentum component brings all Rayleigh rings coming from the pump and idler out of resonance.

Note that the kinematic conditions for OPO are incompatible with the pump and idler being in the subsonic regime. Thus the coupling between the three components always implies some degree of scattering in the signal. In practice, the small value of the signal momentum strongly suppresses its actually visible modulations, something confirmed by the experimental observations.

II. MODEL

The dynamics of polaritons in the OPO regime, and their hydrodynamic properties when scattering against a defect, can be described via a classical driven-dissipative nonlinear Gross-Pitaevskii equation (GPE) for the coupled exciton and cavity fields $\psi_{X,C}(\mathbf{r},t)$ ($\hbar = 1$) [17,28]:

$$i\partial_t \begin{pmatrix} \psi_X \\ \psi_C \end{pmatrix} = \hat{H} \begin{pmatrix} \psi_X \\ \psi_C \end{pmatrix} + \begin{pmatrix} 0 \\ F_p(\mathbf{r},t) \end{pmatrix}. \quad (1)$$

The dispersive X and C fields decay at a rate $\gamma_{X,C}$ and are coupled by the Rabi splitting Ω_R, while the nonlinearity is regulated by the exciton coupling strength g_X:

$$\hat{H} = \begin{pmatrix} \omega^X_{-i\nabla} - i\frac{\gamma_X}{2} + g_X|\psi_X|^2 & \Omega_R/2 \\ \Omega_R/2 & \omega^C_{-i\nabla} - i\frac{\gamma_C}{2} + V_d \end{pmatrix}. \quad (2)$$

We describe the defect via a potential $V_d(\mathbf{r})$ acting on the photonic component; this can either be a defect in the cavity mirror or a localized laser field [25,29,30]. In the conservative, homogeneous, and linear regime [$\gamma_{X,C} =$

$0 = V_d(\mathbf{r}) = g_X$], the eigenvalues of $\hat{H}$ are given by the lower (LP) and upper polariton (UP) energies, $2\omega^{\mathrm{LP,UP}}_{\mathbf{k}} = \omega^C_{\mathbf{k}} + \omega^X_{\mathbf{k}} \mp \sqrt{(\omega^C_{\mathbf{k}} - \omega^X_{\mathbf{k}})^2 + \Omega_R^2}$. The cavity is driven by a continuous-wave laser field $F_p(\mathbf{r},t) = \mathcal{F}_p(\mathbf{r})e^{i(\mathbf{k}_p \cdot \mathbf{r} - \omega_p t)}$ into the OPO regime: Here, polaritons are continuously injected into the pump state with frequency ω_p and momentum $\mathbf{k}_p$, and, above a pump strength threshold, they undergo coherent stimulated scattering into the signal ($\omega_s, \mathbf{k}_s$) and idler ($\omega_i, \mathbf{k}_i$) states.

As a first step, it is useful to get insight into the system behavior in the simple case of a homogeneous pump of strength $\mathcal{F}_p(\mathbf{r}) = f_p$. A numerical study of the coupled equations (1) for the more realistic case of a finite-size top-hat pump profile $\mathcal{F}_p(\mathbf{r})$ will be presented later. To further simplify our analysis, we assume here that the UP dispersion does not get populated by parametric scattering processes, and thus, by means of the Hopfield coefficients $2X^2_{\mathbf{k}}, 2C^2_{\mathbf{k}} = 1 \pm (\omega^C_{\mathbf{k}} - \omega^X_{\mathbf{k}})/\sqrt{(\omega^C_{\mathbf{k}} - \omega^X_{\mathbf{k}})^2 + \Omega_R^2}$, we project the GPE (1) onto the LP component [3,31] $\psi_{\mathbf{k}} = X_{\mathbf{k}}\psi_{X,\mathbf{k}} + C_{\mathbf{k}}\psi_{C,\mathbf{k}}$, where $\psi(\mathbf{r},t) = \sum_{\mathbf{k}} e^{i\mathbf{k}\cdot\mathbf{r}}\psi_{\mathbf{k}}(t)$:

$$i\partial_t \psi_{\mathbf{k}} = \left[\omega^{\mathrm{LP}}_{\mathbf{k}} - i\frac{\gamma_{\mathbf{k}}}{2} \right]\psi_{\mathbf{k}} + C_{\mathbf{k}}\sum_{\mathbf{q}} C_{\mathbf{q}}V_d(\mathbf{k}-\mathbf{q})\psi_{\mathbf{q}}$$

$$+ \sum_{\mathbf{k}_1,\mathbf{k}_2} g_{\mathbf{k},\mathbf{k}_1,\mathbf{k}_2}\psi^*_{\mathbf{k}_1+\mathbf{k}_2-\mathbf{k}}\psi_{\mathbf{k}_1}\psi_{\mathbf{k}_2} + \tilde{f}_p(t)\delta_{\mathbf{k},\mathbf{k}_p}. \quad (3)$$

Here, $\gamma_{\mathbf{k}} = \gamma_X X^2_{\mathbf{k}} + \gamma_C C^2_{\mathbf{k}}$ is the effective LP decay rate, the interaction strength is given by $g_{\mathbf{k},\mathbf{k}_1,\mathbf{k}_2} = g_X X_{\mathbf{k}} X_{\mathbf{k}_1+\mathbf{k}_2-\mathbf{k}} X_{\mathbf{k}_1} X_{\mathbf{k}_2}$, and the pumping term is given by $\tilde{f}_p(t) = C_{\mathbf{k}_p} f_p e^{-i\omega_p t}$. Note that the problem dependence on the exciton-exciton interaction strength g_X can be removed by rescaling both the LP field $\sqrt{g_X}\psi_{\mathbf{k}}(t) \mapsto \psi_{\mathbf{k}}(t)$ and the pump strength $\sqrt{g_X}f_p \mapsto f_p$, something we will do later on to all effects working in terms of energy blueshifts and the rescaled pump intensity.

III. LINEAR-RESPONSE THEORY

In the limit where the homogeneously pumped system is only weakly perturbed by the external potential $V_d(\mathbf{r})$, we apply a linear-response analysis [32]: The LP field is expanded around the mean-field terms for the three $n = 1,2,3 = s,p,i$ OPO states [33],

$$\psi_{\tilde{\mathbf{k}}} = \sum_{n=1}^{3} e^{-i\omega_n t}[\psi_n \delta_{\tilde{\mathbf{k}},0} + u_{n,\tilde{\mathbf{k}}}e^{-i\omega t} + v^*_{n,-\tilde{\mathbf{k}}}e^{i\omega t}], \quad (4)$$

where $\tilde{\mathbf{k}} = \mathbf{k} - \mathbf{k}_n$. Equation (3) is expanded linearly in both the fluctuations terms, $u_{n,\tilde{\mathbf{k}}}$ and $v_{n,\tilde{\mathbf{k}}}$, as well as the defect potential. At zeroth order, the three complex uniform mean-field equations can be solved to obtain the dependence of the signal, pump, and idler energy blueshifts, $\epsilon_n = g_X X^2_{\mathbf{k}_n}|\psi_n|^2$, on the system parameters [31,34]. A typical behavior of ϵ_n as a function of the rescaled pump intensity $I_p = g_X C^2_{\mathbf{k}_p} f^2_p / X^2_{\mathbf{k}_p}$ in the optical limiter regime is plotted in the left panel of Fig. 1. At first order, one obtains six coupled equations diagonal in momentum space [18],

$$\omega \mathbf{w}_{\tilde{\mathbf{k}}} = \mathcal{L}_{\tilde{\mathbf{k}}}\mathbf{w}_{\tilde{\mathbf{k}}} + \frac{1}{2}\mathbf{\Psi}_d, \quad (5)$$
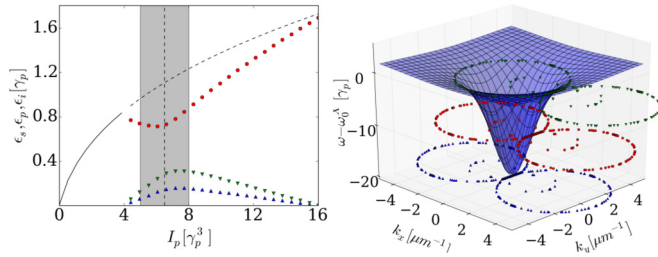
FIG. 1. (Color online) OPO mean-field blueshifts and fluctuation Rayleigh rings in the linear-response scheme for homogeneous pumping. Left panel: signal s [(blue) upper triangles], pump p [(red) circles], and idler i [(green) lower triangles] mean-field energy blueshifts $\epsilon_{n=s,p,i}$ (in units of $\gamma_p = \gamma_{k_p}$) vs the rescaled pump intensity I_p (in units of γ_p^3) in the optical limiter regime. Parameters are $\Omega_R = 5$ meV, zero cavity-exciton detuning, $\gamma_X = \gamma_C = 0.12$ meV, $\omega_p - \omega_0^X = -1.25$ meV, $k_p = 1.6\,\mu\text{m}^{-1}$, $k_s \simeq 0$, and $k_i = 3.2\,\mu\text{m}^{-1}$. The shaded area is the stable OPO region, while the vertical dashed line corresponds to the pump power value chosen for plotting the right panel. Right panel: blueshifted LP dispersion (10) with superimposed Rayleigh curves $\Gamma_{p,i,(u,v),\tilde{k}+k_{p,i}}$ evaluated within the linear-response approximation (same symbols as the left panel). The two rings corresponding to the signal state, $\Gamma_{s,(u,v),\tilde{k}}$, are shrunk to zero because $k_s \simeq 0$.

for the six-component vector $\mathbf{w}_{\tilde{k}} = (u_{n,\tilde{k}}, v_{n,\tilde{k}})^T$ and for the potential part, $\boldsymbol{\Psi}_d = (\psi_n C_{k_n} C_{k+k_n} V_d(\mathbf{k}), -\psi_n^* C_{k_n} C_{k_n-k} V_d(-\mathbf{k}))^T$. In (5) we have only kept the terms oscillating at the frequencies $\omega_n \pm \omega$ and neglected the other terms in the expansion (i.e., $2\omega_n - \omega_m \pm \omega$), which are oscillating at frequencies far from the LP band, and thus with negligible amplitudes. In the particlelike and the holelike channels, the Bogoliubov matrix determining the spectrum of excitations can be written as [18]

$$\mathcal{L}_{\mathbf{k}} = \begin{pmatrix} M_{\mathbf{k}} & Q_{\mathbf{k}} \\ -Q_{-\mathbf{k}}^* & -M_{-\mathbf{k}}^* \end{pmatrix}, \qquad (6)$$

where the three OPO state components are

$$(M_{\mathbf{k}})_{mn} = \left[\omega_{k_m+\mathbf{k}}^{\text{LP}} - \omega_m - i\frac{\gamma_{k_m+\mathbf{k}}}{2} \right]\delta_{m,n}$$
$$+ 2\sum_{q,t=1}^{3} g_{k_m+\mathbf{k},k_n+\mathbf{k},k_t}\psi_q^*\psi_t\delta_{m+q,n+t}, \qquad (7)$$

$$(Q_{\mathbf{k}})_{mn} = \sum_{q,t=1}^{3} g_{k_m+\mathbf{k},k_q,k_t}\psi_q\psi_t\delta_{m+n,q+t}. \qquad (8)$$

In absence of a defect potential ($\boldsymbol{\Psi}_d = 0$), Eq. (5) is the eigenvalue equation for the spectrum of excitations of a homogeneous OPO, i.e., $\det(\mathcal{L}_{\tilde{k}} - \omega) = 0$. The spectrum has six branches, $\omega_{n,(u,v),\tilde{k}}$, labeled by $n = s,p,i$ and (u,v). Even though these degrees of freedom are mixed together, at large momenta, one recovers the LP dispersions shifted by the three states' energies and momenta, i.e.,

$$\lim_{\tilde{k} \gg \sqrt{2m_C\Omega_R}} \omega_{n,(u,v),\tilde{k}} = \pm(\omega_{\mathbf{k}-k_n}^{\text{LP}} - \omega_n), \qquad (9)$$

where $+$ $(-)$ corresponds to the u (v) particlelike (holelike) branch. The OPO solution is stable (shaded area in Fig. 1) as far as $\text{Im}\,\omega_{n,(u,v),\tilde{k}} < 0$.

The shape of the patterns, or Cherenkov-like waves, resulting from the elastic scattering of the OPO 3-fluids against the static ($\omega = 0$) defect can be determined starting from the spectrum, and in particular evaluating the closed curves $\Gamma_{n,(u,v),\tilde{k}}$ in $\mathbf{k}$ space, or "Rayleigh rings" [35] defined by the condition $\text{Re}\,\omega_{n,(u,v),\tilde{k}} = 0$.[1] The modulations propagate with a direction $\hat{\eta}_{n,(u,v),\tilde{k}}$ orthogonal to each curve $\Gamma_{n,(u,v),\tilde{k}}$, a pattern wavelength given by the corresponding $|\tilde{k}|$, and a group velocity $\mathbf{v}_{n,(u,v),\tilde{k}}^{(g)} = \nabla_{\tilde{k}}\text{Re}\,\omega_{n,(u,v),\tilde{k}}$, where $\xi_{n,(u,v),\tilde{k}} = |\mathbf{v}_{n,(u,v),\tilde{k}}^{(g)}|/\text{Im}\,\omega_{n,(u,v),\tilde{k}}|$ determines the distance, at any given direction $\hat{\eta}_{n,(u,v),\tilde{k}}$, over which the perturbation extends away from the defect. For a single fluid under a coherent pump, the qualitative shape of the modulation pattern generated in the fluid by the defect is mostly determined by the excitation spectrum [36,37].

For OPO, the spectrum of excitation on top of each of the three, $n = 1,2,3$, states (see [34]) generates six identical Rayleigh rings $\Gamma_{n,(u,v),\tilde{k}}$ for the three states. The Rayleigh rings for the OPO conditions specified in Fig. 1 are clearly visible in the right panels of Fig. 2, where we plot the $\mathbf{k}$-space photoluminescence filtered at each state energy, i.e., $|\psi_{\tilde{k}}(\omega_n)|^2 = |\psi_n\delta_{\tilde{k},0} + u_{n,\tilde{k}} + v_{n,-\tilde{k}}^*|^2$. We have chosen here a δ-like defect potential, $V_d(\mathbf{k}) = g_d$, but we have checked that our results do not depend on its exact shape [34]. For the OPO conditions considered here, the signal momentum is at $k_s \simeq 0$, and thus only four of the six rings are present. The same rings are also plotted in the right panel of Fig. 1, shifted at each of the three OPO states' momentum k_n, $\Gamma_{n,(u,v),\tilde{k}+k_n}$, and energies ω_n. It is important to note that, even though the three OPO states have locked responses because they display the same spectrum of excitations, only one of the rings $\Gamma_{n,(u,v),\tilde{k}+k_n}$ is the most resonant at ω_n with the interaction blueshifted lower polariton dispersion,

$$\bar{\omega}_{\mathbf{k}}^{\text{LP}} = \omega_{\mathbf{k}}^{\text{LP}} + 2X_{\mathbf{k}}^2\sum_{n=1}^{3}\epsilon_n, \qquad (10)$$

where $\epsilon_n = g_X X_{k_n}^2|\psi_n|^2$ are the mean-field energy blueshifts (measured in Fig. 1 in units of $\gamma_p = \gamma_{k_p}$). This implies that the most visible modulation for each fluid should be the most resonant one, with superimposed weaker modulations coming from the other two state rings.

In the specific case of Fig. 1, the signal is at $k_s \simeq 0$ and thus produces no rings in momentum space. The other four rings are very far from being resonant with the blueshifted LP dispersion (10) at ω_s, and thus the signal displays only an extremely weak modulation coming from the next closer ring, which is the one associated with the pump state, $\Gamma_{p,u,\tilde{k}+k_s}$. We estimate that the signal modulation amplitudes are roughly 1% of the average

---

[1] Even if they do not appear to be relevant here, note that the presence of a nonvanishing imaginary part of the excitation spectrum $\text{Im}\,\omega_{n,(u,v),\tilde{k}} \neq 0$ introduces some complications: Even in the absence of any Rayleigh ring, the drag force can be nonvanishing and the standard Landau criterion may fail to identify a critical velocity [24].
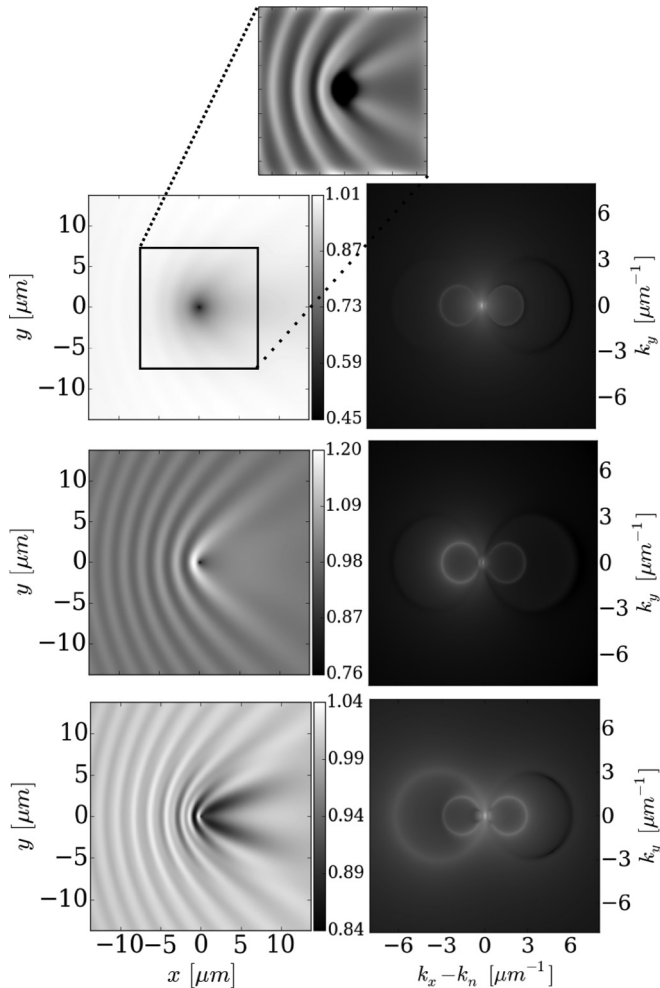
FIG. 2. Linear responses to a static defect of the three OPO states in real and momentum space. Rescaled filtered OPO emissions [signal (top panels), pump (middle), and idler (bottom)] in real space $|\psi(\mathbf{r},\omega_n)|^2/|\psi_n|^2$ (left panels in linear scale) and momentum space $|\psi_{\bar{\mathbf{k}}}(\omega_n)|^2$ (right panel in logarithmic scale) obtained within the linear-response approximation. The OPO parameters are the same as those in Fig. 1, and the strength of the δ-like defect potential, $V_d(\mathbf{k}) = g_d$, is fixed to $g_d = 0.5\gamma_p$ μm^2. For the top left panel of the signal emission in real space, Gaussian filtering is applied to enhance the short-wavelength modulations, the amplitudes of which are otherwise roughly 1% of the average signal intensity and about a factor of 10 times weaker than the modulation amplitudes in the pump fluid.

signal intensity and about a factor of 10 times weaker than the modulation amplitudes in the pump fluid. To show that the signal has weak modulations coming from the pump, we apply a Gaussian filter to the real-space images (see the inset of the top-left panel of Fig. 2). As explained in more detail in [34], Gaussian filtering consists of subtracting from the original data a copy that has been convolved with a Gaussian kernel, thus getting rid of the long-wavelength modulations. This procedure reveals that indeed the pump imprints its modulation also into the signal, even though these are extremely weak, thus leaving the signal basically insensitive to the presence of the defect.

Pump and idler states are each mostly resonant with their own rings, i.e., $\Gamma_{p,u,\bar{\mathbf{k}}+\mathbf{k}_p}$ at ω_p and $\Gamma_{i,u,\bar{\mathbf{k}}+\mathbf{k}_i}$ at ω_i, respectively. Thus one should then observe two superimposed modulations in both pump and idler filtered emissions, the stronger one for each being the most resonant one. However, the modulations associated with the idler only propagate very close to the defect, at an average distance $\bar{\xi}_{i,u,\bar{\mathbf{k}}} \sim 1.7$ μm before getting damped, and thus they are not clearly visible. For the OPO conditions considered, this is due to the small idler group velocity $\mathbf{v}^{(g)}_{i,u,\bar{\mathbf{k}}}$, as the dispersion is almost excitonic at the idler energy.

We can conclude that, for the typical OPO condition with a signal at $k_s \simeq 0$, considered in Figs. 1 and 2, the signal fluid does not show modulations, and the extremely weak scattering inherited from the pump state can be appreciated only after a Gaussian filtering procedure of the image. In contrast, the idler has a locked response to that of the pump state. Note that, for the conditions shown in Fig. 1, as well as the other cases considered in Ref. [34], the subsonic to supersonic crossover of the pump-only state [25] happens well above the region of stability of OPO. Thus it is not possible to study a case in which the pump is already subsonic and at the same time promotes stimulated scattering.

IV. EXPERIMENTS

We now turn to the experimental analysis. We use a continuous-wave laser to drive a high-quality ($Q = 14\,000$) GaAs microcavity sample into the OPO regime—details on the sample can be found in a previous publication [38,39]. The polariton dispersion is characterized by a Rabi splitting $\Omega_R = 5.4$ meV, the exciton energy $\omega_0^X = 1485.26$ meV, and we choose a sample region where the cavity-exciton detuning is slightly negative, -1 meV. We pump at $k_p = 0.89$ μm^{-1} and $\omega_p - \omega_0^X = -2.43$ meV, and, at pump powers 1.5 times above threshold, we obtain an OPO with the signal at small wave vector $k_s = 0.21$ μm^{-1} and $\omega_s - \omega_0^X = -2.95$ meV, and the idler at $k_i = 1.57$ μm^{-1} and $\omega_i - \omega_0^X = -1.91$ meV. The defect we use in the sample is a localized inhomogeneity naturally present in the cavity mirror. Note that the exact location of the defect can be extracted from the emission spectrum, and it is indicated with a dot (orange) symbol in the profiles of Fig. 3.

To filter the emission at the three states energies, $I_{s,p,i}$ ($\mathbf{r} = x, y$), and to obtain 2D spatial maps for the OPO three states, we use a spectrometer and, at a fixed position x_0, obtain the intensity emission as a function of energy and position, $I(\epsilon, x_0, y)$. By changing x_0, we build the full emission spectrum as a function of energy and 2D position, $I(\epsilon, \mathbf{r})$. The filtered emission for each OPO state is obtained from the integrals $I_{n=s,p,i}(\mathbf{r}) = \int_{\omega_n - \sigma}^{\omega_n + \sigma} d\epsilon\, I(\epsilon, \mathbf{r})$, with $\sigma = 0.08$ meV. The results are shown in Fig. 3 for, respectively, the signal (top panel), pump (middle), and idler (bottom) profiles. The signal profile shows no appreciable modulations around the defect locations, nor could any be observed after applying a Gaussian filtering procedure of the image. In contrast, in agreement with the theoretical results, both filtered profiles of the pump and idler show the same Cherenkov-like pattern. We extract the wave crests from the idler profile [(yellow) contours in the bottom panel] and superimpose them to the pump profile (middle
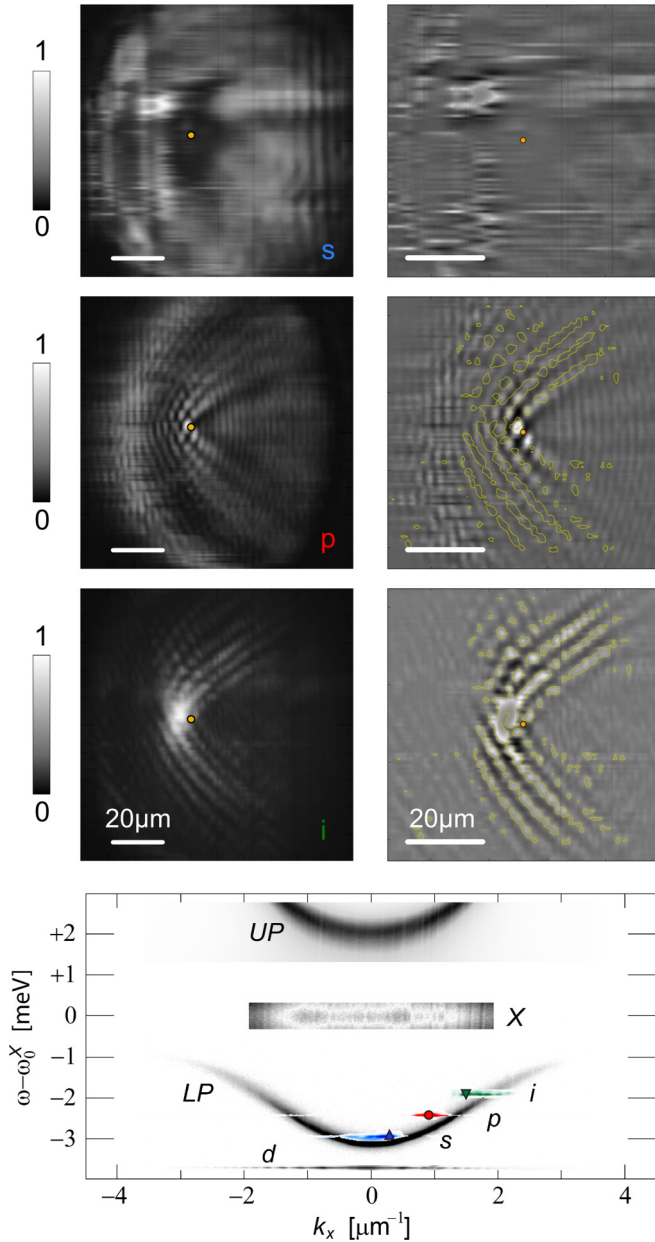
FIG. 3. (Color online) Experimental OPO spectrum and filtered emissions of the signal, pump, and idler in the presence of a structural defect. The six panels show the filtered emission profiles in real space of the signal (top), the pump (middle), and the idler (bottom) $I_{s,p,i}(\mathbf{r})$. A Gaussian filtering to enhance the short-wavelength modulations is applied in the right column panels. Here, the extracted wave crests from the idler emission (yellow contours in the bottom panel) are also superimposed to the pump profile (middle) by applying a π-phase shift. The (orange) dot indicates the position of the defect. The lower panel shows the experimental OPO spectrum. Energy and momentum of the three OPO states are labeled with a (blue) upper triangle (signal), a (red) circle (pump), and a (green) lower triangle (idler), while the localized state, clearly visible just below the bottom of the LP dispersion, is indicated with the symbol d. The bare LP dispersion is extracted from an off-resonant low pump power measurement, as well as the emission of the exciton reservoir (X) and that of the UP dispersion (each in a different scale).

panel) with an added π-phase-shift, revealing that the only modulations visible in the idler state are the ones coming from the pump state.

V. NUMERICAL ANALYSIS

The agreement between the results obtained experimentally and within the linear-response approximation is additionally confirmed by an exact full numerical analysis of the coupled equations (1) for a finite-size pump via a fifth-order adaptive-step Runge-Kutta algorithm. Details are given in [34]. The pumping conditions are very similar to those previously considered in the linear-response approximation of Figs. 1 and 2, while the pump profile $\mathcal{F}_p(\mathbf{r})$ is now a finite-size top
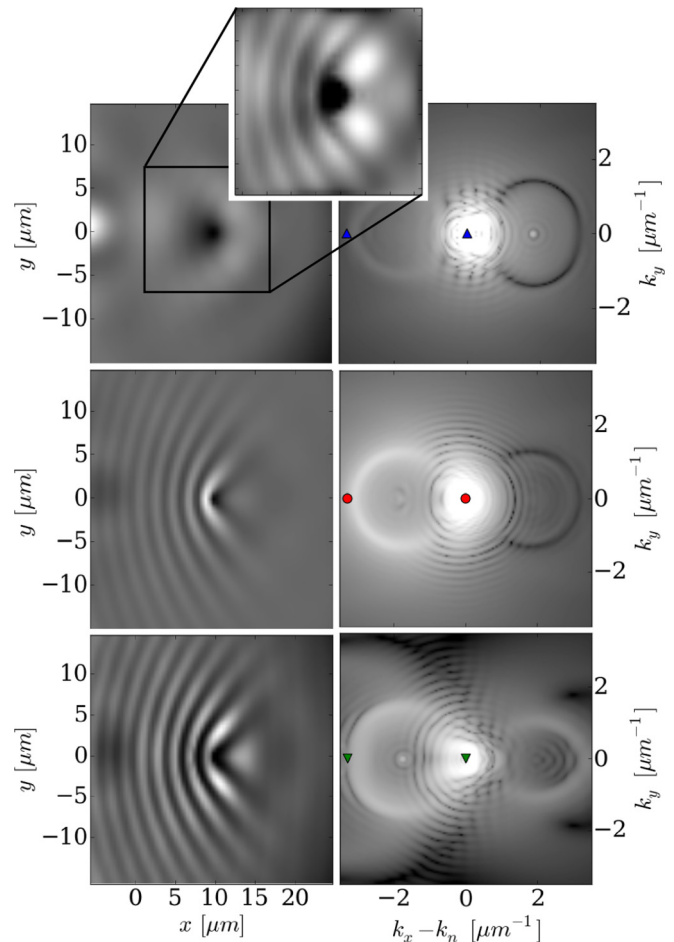

FIG. 4. (Color online) Full numerical responses to a static defect of the three OPO states in real and momentum space. Filtered OPO emissions [signal (top panels), pump (middle), and idler (bottom)] in real space $|\psi_C(\mathbf{r},\omega_n)|^2$ (left panels in linear scale) and momentum space $|\psi_C(\tilde{\mathbf{k}},\omega_n)|^2$ (right panel in logarithmic scale) obtained by a full numerical evaluation of (1). For the top left panel of the signal space emission, Gaussian filtering is applied to enhance the short-wavelength modulations of this state, revealing that the modulations corresponding to the pump state are also imprinted (though weakly) into the signal. The symbols indicate the pump ring diameter extracted from fitting the upstream modulations and resulting in a density-wave wave vector coinciding with that of the pump, $k_p = 1.6 \, \mu\mathrm{m}^{-1}$.

hat. In particular, we consider the case of zero cavity-exciton detuning, $k_p = 1.6 \ \mu\mathrm{m}^{-1}$, $\omega_p - \omega_X^0 = -0.44$ meV, and the pump power strength is fixed just above threshold, so that to produce a stable steady state OPO. This, in absence of the defect, is characterized by a signal at small wavevector $k_s = -0.2 \ \mu\mathrm{m}^{-1}$ and idler at $k_i = 3.4 \ \mu\mathrm{m}^{-1}$.

When adding a localized defect potential, the steady-state OPO develops Rayleigh rings in momentum space, yet, as shown in [34], the spectrum continues to be δ-like in energy, allowing us to easily filter in energy the emission of the three OPO states. The results are shown in Fig. 4, where real-space emissions $|\psi_C(\mathbf{r},\omega_n)|^2$ are plotted in the left panels, while the ones in momentum space $|\psi_C(\tilde{\mathbf{k}},\omega_n)|^2$ are plotted in the right panels. We observe a very similar phenomenology to that obtained in the linear approximation shown in Fig. 2. The signal now is at slightly negative values of momenta $k_s = -0.2 \ \mu\mathrm{m}^{-1}$, thus implying a very small Rayleigh ring associated with this state. Thus we observe that only the modulations associated with the pump are the ones that are weakly imprinted in the signal state and that can be observed by means of a Gaussian filtering (inset of the top-left panel). We have fitted the upstream wave crests and obtained the same modulation wave vector as the pump one [(blue) upper triangles]. Similar to the linear-response case, we also find here that the most visible perturbation in the emission filtered at the idler energy is the one due to the pump Rayleigh ring. As before, the modulations due to the idler Rayleigh ring cannot propagate far from the defect because of the small group velocity associated with this state.

VI. CONCLUSIONS

To conclude, we have reported a joint theoretical and experimental study of the superfluid properties of a nonequilibrium condensate of polaritons in the so-called optical parametric oscillator configuration by studying the scattering against a static defect. We have found that while the signal is basically free from modulations, the pump and idler lock to the same response. We have highlighted the role of the coupling between

the OPO components because of nonlinear and parametric processes. These are responsible for the transfer of the spatial modulations from one component to the other. This process is most visible in the clear spatial modulation pattern that is induced by the nonsuperfluid pump onto the idler, while the same modulations are only extremely weakly transferred into the signal, because of its low characteristic wave vector, so much that experimentally cannot be resolved. The main features of the real- and momentum-space emission patterns are understood in terms of Rayleigh scattering rings for each component and a characteristic propagation length from the defect; the rings are then transferred to the other components by nonlinear and parametric processes.

Much interest has been recently devoted to aspects related to algebraic order [40,41] and superfluid response [42] in driven-dissipative polariton condensates. Our theoretical and experimental results further stress the complexities and richness involved when looking for superfluid behaviors in nonequilibrium multicomponent condensates such as the ones obtained in the optical parametric oscillation regime.

[1] A. V. Kavokin, J. J. Baumberg, G. Malpuech, and F. P. Laussy, *Microcavities* (Oxford University Press, Oxford, 2007).

[2] C. Ciuti, P. Schwendimann, B. Deveaud, and A. Quattropani, Phys. Rev. B **62**, R4825 (2000).

[3] C. Ciuti, P. Schwendimann, and A. Quattropani, Phys. Rev. B **63**, 041303 (2001).

[4] C. Ciuti, P. Schwendimann, and A. Quattropani, Semicond. Sci. Technol. **18**, S279 (2003).

[5] R. M. Stevenson, V. N. Astratov, M. S. Skolnick, D. M. Whittaker, M. Emam-Ismail, A. I. Tartakovskii, P. G. Savvidis, J. J. Baumberg, and J. S. Roberts, Phys. Rev. Lett. **85**, 3680 (2000).

[6] P. G. Savvidis, J. J. Baumberg, R. M. Stevenson, M. S. Skolnick, D. M. Whittaker, and J. S. Roberts, Phys. Rev. Lett. **84**, 1547 (2000).

[7] P. G. Savvidis, J. J. Baumberg, R. M. Stevenson, M. S. Skolnick, D. M. Whittaker, and J. S. Roberts, Phys. Rev. B **62**, R13278 (2000).

[8] J. J. Baumberg, P. G. Savvidis, R. M. Stevenson, A. I. Tartakovskii, M. S. Skolnick, D. M. Whittaker, and J. S. Roberts, Phys. Rev. B **62**, R16247 (2000).

[9] M. Saba, C. Ciuti, J. Bloch, V. Thierry-Mieg, R. André, L. S. Dang, S. Kundermann, A. Mura, G. Bongiovanni, J. L. Staehli, and B. Deveaud, Nature (London) **414**, 731 (2001).

[10] K. Edamatsu, G. Oohata, R. Shimizu, and T. Itoh, Nature (London) **431**, 167 (2004).

[11] S. Savasta, O. DiStefano, V. Savona, and W. Langbein, Phys. Rev. Lett. **94**, 246401 (2005).

[12] L. Lanco, S. Ducci, J.-P. Likforman, X. Marcadet, J. A. W. van Houwelingen, H. Zbinden, G. Leo, and V. Berger, Phys. Rev. Lett. **97**, 173901 (2006).

[13] M. Abbarchi, V. Ardizzone, T. Lecomte, A. Lemaitre, I. Sagnes, P. Senellart, J. Bloch, P. Roussignol, and J. Tignon, Phys. Rev. B **83**, 201310 (2011).

[14] V. Ardizzone, M. Abbarchi, A. Lemaitre, I. Sagnes, P. Senellart, J. Bloch, C. Delalande, J. Tignon, and P. Roussignol, Phys. Rev. B **86**, 041301 (2012).

[15] W. Xie, H. Dong, S. Zhang, L. Sun, W. Zhou, Y. Ling, J. Lu, X. Shen, and Z. Chen, Phys. Rev. Lett. **108**, 166401 (2012).

[16] T. Lecomte, V. Ardizzone, M. Abbarchi, C. Diederichs, A. Miard, A. Lemaitre, I. Sagnes, P. Senellart, J. Bloch, C. Delalande, J. Tignon, and P. Roussignol, Phys. Rev. B **87**, 155302 (2013).

[17] I. Carusotto and C. Ciuti, Rev. Mod. Phys. **85**, 299 (2013).

[18] M. Wouters and I. Carusotto, Phys. Rev. A **76**, 043807 (2007).

[19] D. Sanvitto, F. Marchetti, M. Szymańska, G. Tosi, M. Baudisch, F. Laussy, D. Krizhanovskii, M. Skolnick, L. Marrucci, A. Lemaitre, J. Bloch, C. Tejedor, and L. V. na, Nat. Phys. **6**, 527 (2010).

[20] F. M. Marchetti, M. H. Szymańska, C. Tejedor, and D. M. Whittaker, Phys. Rev. Lett. **105**, 063902 (2010).

[21] F. M. Marchetti and M. H. Szymańska, *Exciton Polaritons in Microcavities: New Frontiers*, in *Vortices in Polariton OPO Superfluids* (Springer-Verlag, Berlin, 2012).

[22] A. J. Leggett, Rev. Mod. Phys. **71**, S318 (1999).

[23] J. Kasprzak, M. Richard, S. Kundermann, A. Baas, P. Jeanbrun, J. M. J. Keeling, F. M. Marchetti, M. H. Szymańska, R. André, J. L. Staehli, V. Savona, P. B. Littlewood, B. Devaud, and L. S. Dang, Nature (London) **443**, 409 (2006).

[24] M. Wouters and I. Carusotto, Phys. Rev. Lett. **105**, 020602 (2010).

[25] A. Amo, J. Lefrère, S. Pigeon, C. Adrados, C. Ciuti, I. Carusotto, R. Houdré, E. Giacobino, and A. Bramati, Nat. Phys. **5**, 805 (2009).

[26] A. Amo, D. Sanvitto, F. P. Laussy, D. Ballarini, E. del Valle, M. D. Martin, A. Lemaitre, J. Bloch, D. N. Krizhanovskii, M. S. Skolnick, C. Tejedor, and L. V. Na, Nature (London) **457**, 291 (2009).

[27] M. H. Szymanska, F. M. Marchetti, and D. Sanvitto, Phys. Rev. Lett. **105**, 236402 (2010).

[28] D. M. Whittaker, Phys. Status Solidi C **2**, 733 (2005).

[29] A. Amo, S. Pigeon, C. Adrados, R. Houdré, E. Giacobino, C. Ciuti, and A. Bramati, Phys. Rev. B **82**, 081301 (2010).

[30] J. M. Zajac and W. Langbein, Phys. Rev. B **86**, 195401 (2012).

[31] M. Wouters and I. Carusotto, Phys. Rev. B **75**, 075332 (2007).

[32] G. E. Astrakharchik and L. P. Pitaevskii, Phys. Rev. A **70**, 013608 (2004).

[33] D. M. Whittaker, Phys. Rev. B **71**, 115301 (2005).

[34] See Supplemental Material at http://link.aps.org/supplemental/10.1103/PhysRevB.92.035307 for details on the model, used parameters, and numerical procedures.

[35] I. Carusotto and G. Rousseaux, in *Analogue Gravity Phenomenology*, Lecture Notes in Physics, Vol. 870, edited by D. Faccio, F. Belgiorno, S. Cacciatori, V. Gorini, S. Liberati, and U. Moschella (Springer International Publishing, Switzerland, 2013), pp. 109–144.

[36] I. Carusotto, S. X. Hu, L. A. Collins, and A. Smerzi, Phys. Rev. Lett. **97**, 260403 (2006).

[37] I. Carusotto and C. Ciuti, Phys. Rev. Lett. **93**, 166401 (2004).

[38] D. Ballarini, M. D. Giorgi, E. Cancellieri, R. Houdré, E. Giacobino, R. Cingolani, A. Bramati, G. Gigli, and D. Sanvitto, Nat. Commun. **4**, 1778 (2013).

[39] L. Dominici, D. Colas, S. Donati, J. P. Restrepo Cuartas, M. De Giorgi, D. Ballarini, G. Guirales, J. C. López Carreño, A. Bramati, G. Gigli, E. del Valle, F. P. Laussy, and D. Sanvitto, Phys. Rev. Lett. **113**, 226401 (2014).

[40] E. Altman, L. M. Sieberer, L. Chen, S. Diehl, and J. Toner, Phys. Rev. X **5**, 011017 (2015).

[41] G. Dagvadorj, J. M. Fellows, S. Matyjaskiewicz, F. M. Marchetti, I. Carusotto, and M. H. Szymanska, arXiv:1412.7361.

[42] J. Keeling, Phys. Rev. Lett. **107**, 080402 (2011).